Preparation, thermal properties, and structures of ionic plastic crystals with sandwich and half-sandwich Ru complexes

Inoue, Ryota

Sumitani, Ryo

Mochida, Tomoyuki

Journal of Organometallic Chemistry 1013 (2024) 123162

Contents lists available at ScienceDirect

Journal of Organometallic Chemistry

journal homepage: www.elsevier.com/locate/jorganchem

Preparation, thermal properties, and structures of ionic plastic crystals with sandwich and half-sandwich Ru complexes

Ryota Inoue [a], Ryo Sumitani [a], Tomoyuki Mochida [a,b,*]

[a] Department of Chemistry, Graduate School of Science, Kobe University, 1-1 Rokkodai, Nada, Kobe, Hyogo 657-8501, Japan
[b] Research Center for Membrane and Film Technology, Kobe University, 1-1 Rokkodai, Nada, Kobe, Hyogo 657-8501, Japan

ARTICLE INFO

Keywords:
Sandwich complexes
Half-sandwich complexes
Phase transitions
Ionic plastic crystals
Thermal properties
Crystal structures

ABSTRACT

We have recently been investigating the phase behavior of salts of cationic sandwich complexes in pursuit of novel ionic plastic crystals (IPCs). In this study, we synthesized salts containing sandwich complexes [Ru(Cp)(C_6H_6)]X ([**1**]X; X = CPFSA$^-$ (1,1,2,2,3,3-hexafluoropropane-1,3-disulfonimide), $SbCl_6^-$) and half-sandwich complexes [Ru(Cp)$(DMSO)_3$]X ([**2**]X; X = CPFSA$^-$, FSA$^-$ ($(FSO_2)_2N^-$), PF_6^-). In addition, we examined their thermal properties and crystal structures. Among them, [**1**]CPFSA exhibited an IPC phase between 365 and 630 K, whereas the others did not undergo phase transitions at 123–403 K. The cations and anions were alternately arranged in the crystals of [**1**]X, whereas [**2**]X did not exhibit the alternating arrangement except for [**2**]PF_6. The results showed that alternating molecular arrangements are crucial for the IPC formation, although low symmetry of the ion environment and intermolecular steric hindrance may inhibit it.

1. Introduction

Ionic plastic crystals (IPCs) have recently been intensively studied for their application in solid electrolytes [1]. An IPC phase is a solid–liquid intermediate phase characterized by nearly globular molecules, where the molecular center of gravity is ordered but the molecular orientation is disordered, thereby allowing for isotropic molecular rotation. Extensive research has been conducted on the ionic conductivity, dielectric properties, and thermal properties of IPCs [1–15]. Most salts with an IPC phase are quaternary ammonium salts. However, the salts of sandwich complexes, such as those derived from ferrocene, exhibit an IPC phase because of the globular shape of their molecules, although their phase transition temperatures into the IPC phase are typically higher than room temperature [16–18]. To investigate organometallic IPCs, we studied the phase behaviors of salts containing cationic sandwich complexes to determine the correlation between the molecular shape, volume, and phase transition temperature [19–26]. We observed that the transition temperature of [Fe(C_5Me_5)$_2$]X (X = anion) tended to decrease with an increase in anion volume [25], whereas the opposite was the case for [Ru(Cp)(C_6H_6)]X ([**1**]X; Cp = C_5H_5) [19]. In salts exhibiting an IPC phase, the cations and anions are alternately arranged in the ordered phase; however, salts lacking this alternating structure generally do not exhibit an IPC phase [19,22,23,25,26].

This study aimed to investigate IPC phases in sandwich and half-sandwich complexes to determine the structural requirements for IPCs. While half-sandwich complexes are another category of useful organometallic complexes, their IPC phases remain unexplored. Two salts of cationic sandwich Ru complexes ([**1**]X; X = CPFSA$^-$, $SbCl_6^-$; Fig. 1a) were synthesized in this study. Previous reports have indicated that [**1**]PF_6 and [**1**]FSA (FSA$^-$ = $(FSO_2)_2N^-$) exhibit an IPC phase [26,27]. In addition, the salts of a dimethyl sulfoxide (DMSO)-coordinated half-sandwich CpRu complex with the same anion ([**2**]X; X = CPFSA$^-$, FSA$^-$, PF_6^-) were synthesized, although the salt with $SbCl_6^-$ was not obtained. Differential scanning calorimetry (DSC), thermogravimetry-differential thermal analysis (TG-DTA), and crystal structure analysis were performed. Fig. 1b summarizes the cation–anion arrangements and IPC formation found in [**1**]X and [**2**]X, including those reported for [**1**]PF_6 and [**1**]FSA; the half-sandwich complexes [**2**]X did not exhibit an IPC phase. Following these results, the effects of molecular and crystal structures on IPC formation are discussed.

2. Results and discussion

2.1. Preparation and phase behavior

[**1**]CPFSA and [**1**]$SbCl_6$ were synthesized through anion exchange of

* Corresponding author.
E-mail address: tmochida@platinum.kobe-u.ac.jp (T. Mochida).

https://doi.org/10.1016/j.jorganchem.2024.123162
Received 5 March 2024; Received in revised form 11 April 2024; Accepted 27 April 2024
Available online 28 April 2024

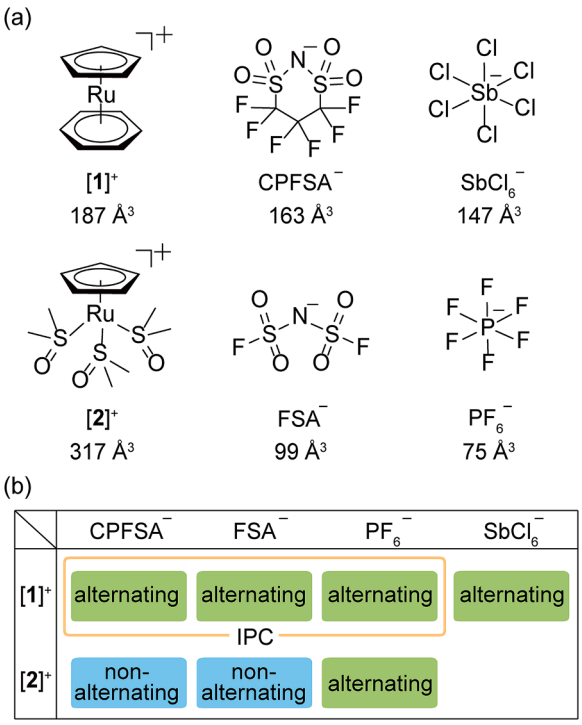

Fig. 1. (a) Structures of the cations and anions used in this study. The molecular volumes estimated by DFT calculations are shown for each molecule. (b) Cation–anion arrangements and IPC formation in [**1**]X and [**2**]X.

[**1**]Cl and the reaction of [**1**]Cl with $SbCl_5$, respectively (74% and 78% yield). [**2**]PF_6 was synthesized by reacting $[Ru(Cp)(CH_3CN)_3]PF_6$ with DMSO (70% yield). [**2**]X (X = $CPFSA^-$, FSA^-) were obtained by UV irradiation of a DMSO solution of [**1**]X (43% and 58% yield). These salts were colorless to pale-yellow solids. [**2**]$SbCl_6$ could not be obtained using the same method, as the photoirradiation of [**1**]$SbCl_6$ produced decomposition products.

DSC measurements were conducted for [**1**]X (X = $CPFSA^-$, $SbCl_6^-$) and [**2**]X (X = $CPFSA^-$, FSA^-, PF_6^-). [**1**]CPFSA underwent a phase transition to an IPC phase, whereas the other salts did not undergo any phase transitions at 123–403 K. The phase transition of [**1**]CPFSA from the low-temperature phase into an IPC phase occurred at 364.8 K (ΔH = 14.9 kJ mol^{-1}, ΔS = 43.5 J mol^{-1} K^{-1}), and the DSC trace is shown in Fig. S1. The IPC phase was confirmed by the loss of birefringence observed via polarized optical microscopy (Fig. S2) and powder X-ray diffraction (PXRD). Fig. 2 shows the PXRD patterns of [**1**]CPFSA at 293 K (low-temperature phase) and 383 K (IPC phase); the latter phase

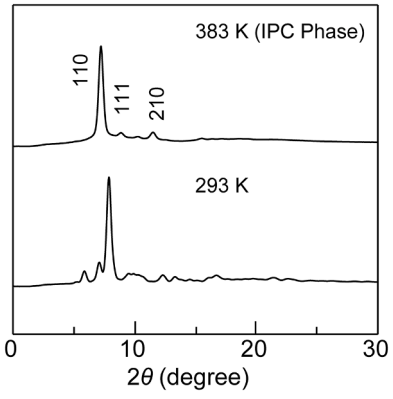

Fig. 2. PXRD patterns of [**1**]CPFSA at 293 K (low-temperature phase) and 383 K (IPC phase) (MoKα).

demonstrated a CsCl-type structure with a strong 110 peak. The high-symmetry structure is characteristic of IPCs [15]. The radius ratio ($\rho = r^-/r^+$) of [**1**]CPFSA is 0.95. Therefore, the structure aligns with the radius ratio rule, which predicts a CsCl-type structure for ionic crystals with $\rho > 0.73$ [28]. The lattice constant determined from the PXRD pattern (7.976(9) Å) corresponded to that estimated from the molecular volume (8.20 Å).

Table 1 lists the phase transition temperatures to the IPC phase (T_c) of [**1**]X (X = $CPFSA^-$, FSA^- [26], and PF_6^- [27]). Despite its larger anion volume, the transition temperature of [**1**]CPFSA is approximately 30 K higher than that of [**1**]PF_6 (T_c = 332.4 K [27]), whereas [**1**]FSA exhibits a considerably higher transition temperature (T_c = 455.8 K [26]). These tendencies are likely correlated with the local symmetry of the ion environment and intermolecular steric hindrance, as discussed below.

2.2. Thermal decomposition behavior

The thermal decomposition behavior of the synthesized salts was investigated by TG-DTA in a nitrogen atmosphere at a sweep rate of 3 K min^{-1} (Fig. 3). [**1**]CPFSA decomposed at a high temperature, whereas the other salts decomposed at lower temperatures upon melting.

The decomposition temperatures (T_{dec}, −3% mass loss temperature) of [**1**]CPFSA and [**1**]$SbCl_6$ were 630 and 495 K, respectively. The decomposition temperature of the former was comparable to those of other CpRu complexes (e.g., [**1**]PF_6: T_{dec} = 630 K [27]). Therefore, this salt exhibits an IPC phase over a wide temperature range from 365 K to above 600 K. The decomposition temperature of [**1**]$SbCl_6$ was considerably low, probably owing to the decomposition occurring upon melting, which might have induced the reaction of the anion. In the DTA curve of [**1**]$SbCl_6$, an endothermic melting peak was observed at 503 K near the decomposition temperature (Fig. S3).

The decomposition temperatures of [**2**]X (X = $CPFSA^-$, FSA^-, PF_6^-) were 431, 438, and 464 K, respectively, which were below 500 K owing to the loss of DMSO ligands in the cation. Although half-sandwich complexes are often reactive and thermally unstable, the results show that the DMSO-coordinated CpRu complex is thermally stable. The decomposition of these salts begins upon melting, as observed visually and by DTA (Fig. S3). The decomposition of [**2**]CPFSA and [**2**]FSA occurred stepwise; the mass loss in the first step corresponded to the loss of one DMSO ligand in each case. For [**2**]CPFSA, the mass loss at 430–460 K (−7 wt%) corresponded to the loss of one DMSO ligand (calculated loss: −11 wt%), and the mass loss within 460–530 K (−27 wt %) corresponded to the loss of the remaining two DMSO ligands (calculated loss: −23 wt%). For [**2**]FSA, the mass loss at 430–460 K (−14 wt%) corresponded to the loss of one DMSO ligand (calculated loss: −14 wt%), and the mass loss within 460–580 K (−53 wt%) corresponded to the loss of the remaining DMSO ligands and the Cp rings (calculated loss: −52 wt%). Although these salts underwent gradual decomposition above the melting point, [**2**]PF_6 decomposed upon melting at a higher temperature. This resulted in a one-step mass loss at 460–540 K (−51 wt %), corresponding to the loss of three DMSO ligands and a Cp ring (calculated loss: −53 wt%).

2.3. Molecular arrangements at low temperature

To determine the correlation between structure and IPC formation, X-ray structural analyses of [**1**]X (X = $CPFSA^-$, $SbCl_6^-$) and [**2**]X (X = $CPFSA^-$, FSA^-, PF_6^-) were performed at 90 K. Details are discussed in the next section. Table 1 includes radius ratios calculated from the molecular volume, structural classification, and coordination number (CN), defined as the number of anions surrounding the cation [29].

The anion arrangements around the cations in [**1**]X and [**2**]X, as determined from the X-ray structures, are displayed in Fig. 4, where only the centers of the cations and anions are shown. [**1**]X and [**2**]PF_6 exhibited alternating cation–anion arrangements in their crystals (Fig. 4a), whereas [**2**]CPFSA and [**2**]FSA exhibited nonalternating

Table 1
Phase transition temperatures to the IPC phase (T_c), thermal decomposition temperatures (T_{dec}), radius ratios (ρ), molecular arrangements, coordination numbers (CN), cation–anion distances (r), average values of r (r_{av}), and standard deviations of r (Δr) for [**1**]X and [**2**]X.

	T_c (K)	T_{dec} (K)	ρ[c]	structure	CN	r (Å)	r_{av} (Å)	Δr
[**1**]CPFSA	364.8	630	0.95	alternating	8	5.90–7.41	6.70	0.57
[**1**]FSA[a]	455.8	570	0.81	alternating	8	5.47–7.38	6.32	0.86
[**1**]PF_6[b]	332.4	630	0.74	alternating	8	5.84–6.21[e] 5.30–6.25[f]	6.05[e] 5.82[f]	0.11[e] 0.37[f]
[**1**]$SbCl_6$	–[d]	495	0.92	alternating	8	5.81–7.61	6.45	0.78
[**2**]CPFSA	–[d]	431	0.80	nonalternating				
[**2**]FSA	–[d]	438	0.68	nonalternating				
[**2**]PF_6	–[d]	464	0.62	alternating	6	5.68–7.58[e] 5.62–7.38[f]	6.64[e], 6.54[f]	0.73[e], 0.64[f]

[a] Ref. [26].
[b] Ref. [27].
[c] Calculated from molecular radii estimated via DFT calculations.
[d] IPC phase was not observed.
[e] Cation I.
[f] Cation II.

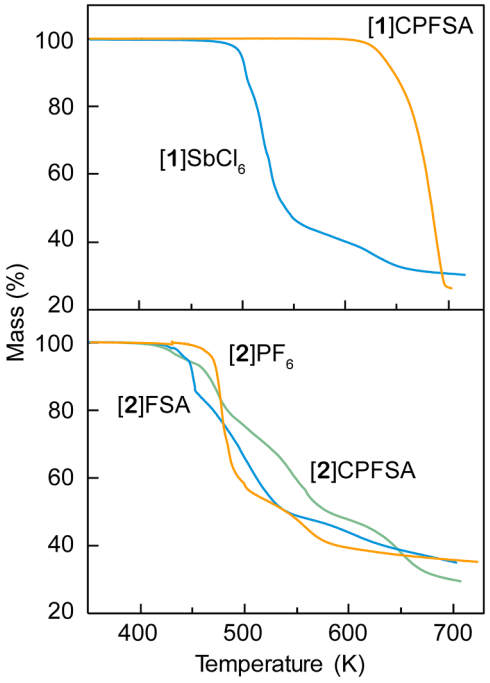

Fig. 3. Thermogravimetric traces of [**1**]X and [**2**]X (3 K min^{-1}, nitrogen atmosphere).

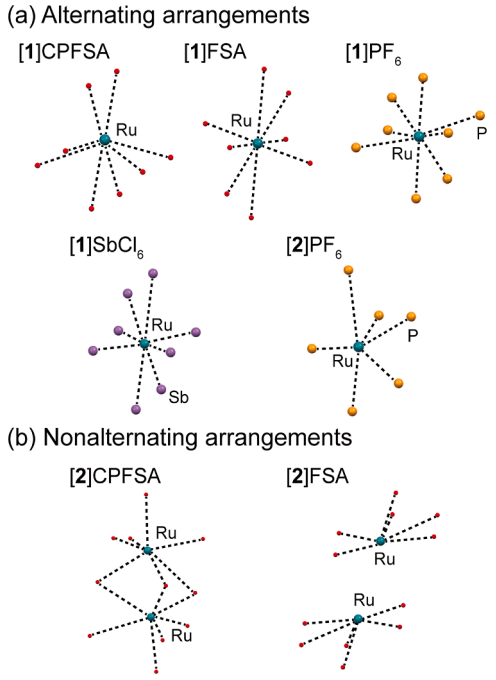

Fig. 4. Anion arrangements around cations in (a) salts with alternating cation–anion arrangements ([**1**]CPFSA, [**1**]FSA [26], [**1**]PF_6 [27], [**1**]$SbCl_6$, and [**2**]PF_6) and (b) those with nonalternating arrangements ([**2**]CPFSA and [**2**]FSA) at 90 K. The centers of the cations and anions are represented as spheres.

structures with partial contacts between the cations (Fig. 4b). The CNs of the salts with the alternating cation–anion arrangement, as determined by the structure analysis, aligned with the radius ratio rule (CN = 8 and 6 for $\rho > 0.73$ and $\rho < 0.73$, respectively; Table 1).

To discuss the effect of the symmetry of the ion environments in these salts, we listed the distances (r) between the centers of the cation and the surrounding anions, their average values (r_{av}), and their standard deviations ($\Delta r = [\sum(r–r_{av})^2/CN]^{1/2}$) in Table 1. The Δr values for [**1**]FSA, [**1**]CPFSA, and [**1**]PF_6 were 0.78, 0.57, and 0.37–0.11, respectively, showing a decreasing trend. In addition, their phase transition temperatures (T_c) decreased in the same order: 455.8 K [26], 364.8 K, and 332.4 K [27], respectively. The correlation appears reasonable; a smaller Δr indicates a uniform arrangement of anions around the cation, which likely facilitates a transition to the IPC phase at lower temperatures due to structural similarities. The average cation–anion distances (r_{av}) changed according to the size of the anion and cation, but the transition temperatures (T_c) did not correlate with r_{av} or the nearest cation–anion distances in these salts. The Δr values for [**1**]$SbCl_6$ and [**2**]PF_6, which did not exhibit the IPC phase, were relatively high (0.78 and 0.73–0.64, respectively). However, their values remained lower than those of [**1**]FSA, suggesting that their local structures, causing intermolecular steric hindrance, are also significant in inhibiting the IPC phase, as discussed below.

2.4. Crystal structures of each salt at low temperature

The individual X-ray structures of [**1**]X (X = $CPFSA^-$, $SbCl_6^-$) and [**2**]X (X = $CPFSA^-$, FSA^-, PF_6^-) at 90 K are discussed in this section. All DMSO ligands in [**2**]X exhibited *S*-coordination structures, as observed in other DMSO-coordinated CpRu complexes [30–32].

Fig. 5a shows the crystal structure of [**1**]CPFSA. This salt crystallized in space group $P2_1/c$ ($Z = 4$); its CN was 8. A pair of a cation and an anion was crystallographically independent, forming an ionic pair (Ru···N = 4.602(2) Å), as observed in cobaltocenium salts with $CPFSA^-$ and other anions [22]. The CPFSA anion exhibited a chair conformation.

Fig. 5b shows the crystal structure of [**1**]$SbCl_6$. This salt crystallized in space group $P2_1/n$ ($Z = 4$), exhibiting an alternating cation–anion arrangement with a CN of 8. One cation and two anions (anions I and II)

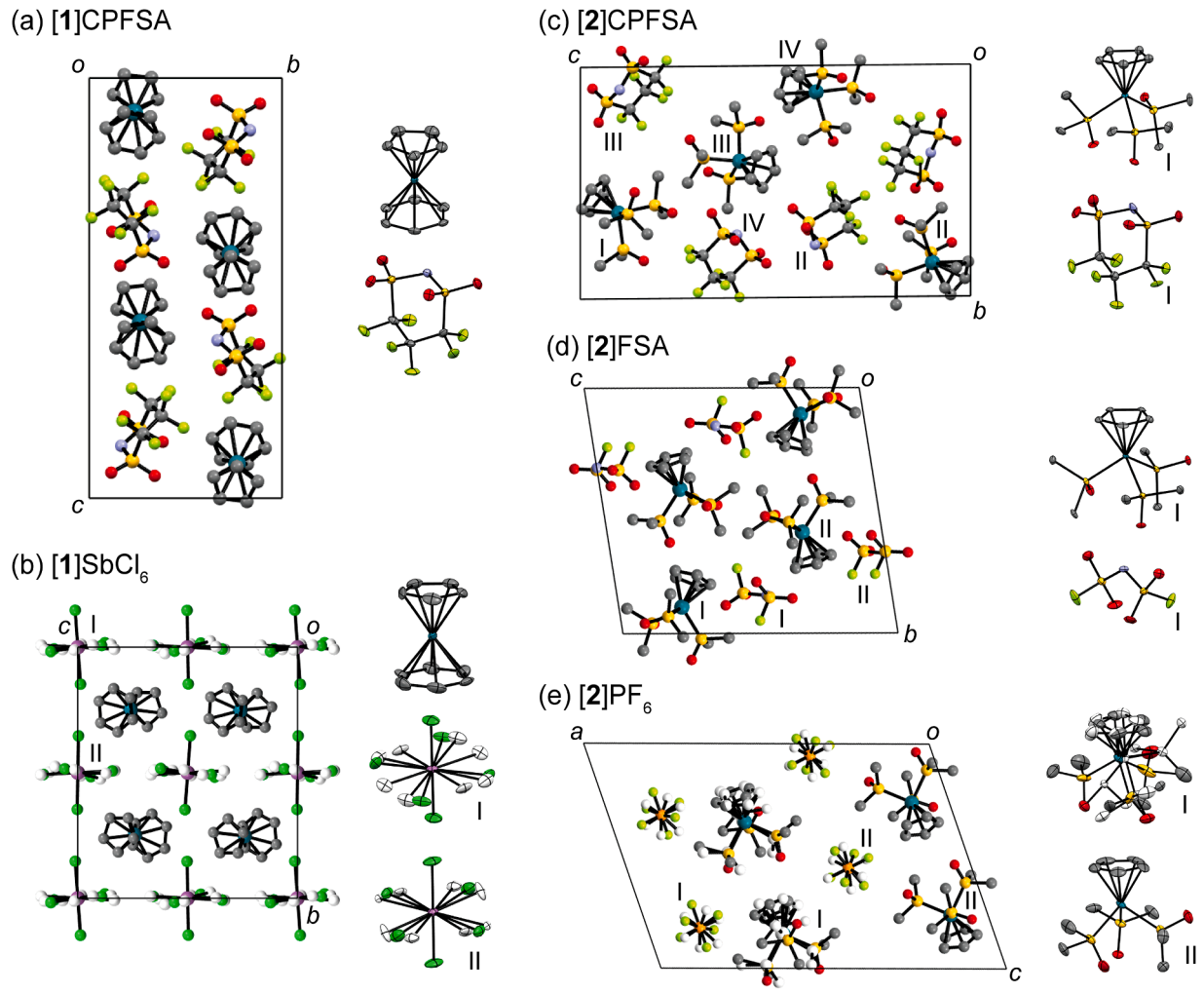

Fig. 5. Crystal structures of (a) [**1**]CPFSA, (b) [**1**]$SbCl_6$, (c) [**2**]CPFSA, (d) [**2**]FSA, and (e) [**2**]PF_6 at 90 K. Only one or two crystallographically independent molecules are shown in the form of ORTEP drawings for each compound. Hydrogen atoms are omitted, and lower occupancy portions of the disordered moieties are indicated by white spheres.

were crystallographically independent. Both anions exhibited uniaxial threefold rotational disorder (occupancy 0.210(3):0.340(3):0.450(3) and 0.175(3):0.293(3):0.532(3)), with the two axial Cl atoms fitting into the cavity between the cations, thereby enabling uniaxial rotation. Although the packing structure of [**1**]$SbCl_6$ was similar to that of [**1**]PF_6 (space group $Pna2_1$, CN 8 [27]), it did not exhibit an IPC phase. This is probably owing to the local anion–cation interlocked structure, which prevents isotropic rotation of the constituent molecules.

Fig. 5c and 5d show the crystal structures of [**2**]CPFSA and [**2**]FSA, respectively. Both salts crystallized in space group $P\bar{1}$. The cations and anions in these salts did not exhibit an alternating arrangement, with the cations being adjacent and exhibiting an interlocked structure. This structure, which is due to the asymmetric cation structure, is probably responsible for the absence of an IPC phase. [**2**]CPFSA contained four crystallographically independent cations and anions, each practically exhibiting the same structure ($Z = 8$), and the CPFSA anion exhibited a chair conformation. [**2**]FSA contained two crystallographically independent cations and anions ($Z = 4$), and the structures of the cations were practically identical. However, anions I and II exhibited *transoid* and *cisoid* conformations, respectively, where *transoid* denotes that the two F atoms are on opposite sides and *cisoid* denotes that they are on the same side relative to the plane defined by the S–N–S bonds [33]. Similar to [**1**]CPFSA, the adjacent cations and anions formed ion pairs in both salts ([**2**]CPFSA, Ru···$N = 4.726$–4.982 Å; [**2**]FSA, Ru···$N = 5.126$–5.381 Å).

Fig. 5e shows the crystal structure of [**2**]PF_6. Contrary to [**2**]CPFSA and [**2**]FSA, this salt exhibited an alternating arrangement of cations and anions ($Z = 4$) with a CN of 6. The structure contained two crystallographically independent cations and anions. Cation II was ordered, whereas cation I was extensively disordered, with twofold disorders of the CpRu moiety (occupancy 0.561(7):0.439(7)) and DMSO ligands (occupancy 0.789(3):0.211(3), 0.768(3):0.232(3), 0.554(17):0.446(17)). Both anions exhibited rotational disorder over two sites (occupancy 0.685(6):0.315(6), and 0.659(7):0.341(7)). The absence of the IPC phase in [**2**]PF_6, despite its alternating arrangement structure, is probably attributed to its local structure. The cations were in contact with each other due to the small anion, resulting in a cation–cation and cation–anion interlocked structure, which likely prevents molecular rotation. The extensive disorder observed in this salt is intriguing, suggesting that a dynamic phase might be induced through the choice of ligands in half-sandwich complexes. However, the current salt did not undergo a phase transition to a rotational phase or an IPC phase, even at high temperatures.

3. Conclusion

We synthesized several salts containing cationic sandwich or half-sandwich CpRu complexes and investigated their molecular arrangements and IPC formation. The results suggest that the symmetry of ionic

environments and the local structural features is essential for IPC formation. Alternating molecular arrangements are crucial for the IPC formation, and deviations from the ideal isotropic cation–anion arrangement tend to increase the transition temperature. [**1**]$SbCl_6$ and [**2**]PF_6 did not exhibit an IPC phase despite their alternating cation–anion arrangement, due to steric hindrance from interlocked molecular arrangements. [**2**]CPFSA and [**2**]FSA exhibited nonalternating cation–anion arrangements, leading to the absence of an IPC phase. These results indicate that half-sandwich complexes are less likely to form IPCs due to their less symmetrical and spherical structures compared to sandwich complexes. The extensive cation disorder observed in [**2**]PF_6 is intriguing, though this salt did not undergo a phase transition to a rotational or an IPC phase. IPCs containing half-sandwich complexes remain undiscovered; therefore, our laboratory is working on using various cations to achieve this and broaden IPC applications.

4. Experimental

4.1. General

[**1**]PF_6 and [**1**]Cl were synthesized according to the literature [26,27]. Other reagents were purchased from TCI or Sigma-Aldrich. UV photoirradiation was performed using a Hamamatsu LC-L1V3 Lightningcure UV–LED lamp (365 nm, 650 mW cm^{-2}). ^{1}H NMR spectra were recorded using a Bruker Avance 400 spectrometer. FT-IR spectra were recorded using a Thermo Scientific Nicolet iS5 FT-IR spectrometer equipped with an attenuated total reflectance attachment (diamond). DSC was performed using a TA Instruments Q100 at a sweep rate of 10 K min^{-1}. The samples were placed in aluminum hermetic pans. A Japan High-Tech 10,013 L cooling and heating stage was used for variable temperature microscopic observations. TG measurements were performed using a Rigaku TG8120 at a rate of 3 K min^{-1} under nitrogen atmosphere. PXRD patterns were recorded using a Bruker APEX II Ultra diffractometer (X-ray source: MoKα). The lattice constants of [**1**]CPFSA at 383 K (IPC phase) were determined using Rigaku PDXL software [34]. DFT calculations were performed using Spartan'20 (Wavefunction Inc.) at the ωB97-D/LanL2DZ level. The molecular radii were estimated from their van der Waals volumes, assuming that the spheres had the same volume as the molecules.

4.2. Synthesis

4.2.1. *[1]CPFSA*

An aqueous solution (3 mL) of Li[CPFSA] (108 mg, 0.36 mmol) was mixed with a methanol solution (2 mL) of [**1**]Cl (68 mg, 0.24 mmol) and stirred for 10 min. The solution was concentrated under reduced pressure and extracted five times using dichloromethane. The organic layer was washed with water and dried over anhydrous magnesium sulfate. The product was reprecipitated by adding diethyl ether to an acetone solution of the product and storing it at −40 °C, resulting in a white solid (103 mg, 74% yield). ^{1}H NMR (400 MHz, $CDCl_3$): δ = 5.46 (s, 5H, Cp-H_5), 6.20 (s, 6H, Ar-H_6). FT-IR (cm^{-1}): 600, 647, 674, 797, 832, 905, 994, 1036, 1090, 1144, 1221, 1260, 1283, 1337, 1352, 1418, 1445, 3111. Anal. Calcd. for $C_{14}H_{11}F_6NO_4S_2Ru$: C, 31.35; H, 2.07; N, 2.61. Found: C, 31.28; H, 1.74; N, 2.52.

4.2.2. *[1]$SbCl_6$*

A solution of $SbCl_5$ (109 mg, 0.36 mmol) in dichloromethane (15 mL) was added to [**1**]Cl (72 mg, 0.26 mmol) and stirred for 1 h in an argon atmosphere. The supernatant was removed, and the precipitate was washed thrice with dichloromethane. The product was collected by filtration and recrystallized from acetone–diethyl ether (−40 °C) to afford the desired product as pale-yellow crystals (116 mg, 78% yield). ^{1}H NMR (400 MHz, CD_3CN): δ = 5.37 (s, 5H, Cp-H_5), 6.12 (s, 6H, Ar-H_6). FT-IR (cm^{-1}): 828, 855, 1001, 1005, 1109, 1151, 1414, 1441, 3084, 3111. Anal. Calcd. for $C_{11}H_{11}Cl_6RuSb$: C, 22.83; H, 1.92; N, 0.00. Found: C, 22.72; H, 1.43; N, 0.06.

4.2.3. *[2]X (X = CPFSA, FSA)*

A solution of [**1**]CPFSA (27 mg, 0.05 mmol) in DMSO (0.3 mL) was irradiated with UV light (365 nm, LED) for 29 h at ambient temperature in a nitrogen atmosphere. The solvent was evaporated and dried under vacuum at 80 °C. The product was reprecipitated by adding diethyl ether to an acetone solution of the product and stored at −40 °C, and the procedure was repeated thrice to afford the desired product as a pale-yellow solid (15 mg, 43% yield). ^{1}H NMR (400 MHz, $CDCl_3$): δ = 3.54 (s, 18H, S(CH_3)$_2$), 5.33 (s, 5H, Cp-H_5). FT-IR (cm^{-1}): 573, 604, 677, 712, 797, 847, 905, 997, 1017, 1028, 1090, 1121, 1152, 1221, 1283, 1352, 1418, 2926, 3011, 3103. Anal. Calcd. for $C_{14}H_{23}F_6NO_7RuS_5$: C, 24.28; H, 3.35; N, 2.02. Found: C, 24.35; H, 3.41; N, 1.96.

[**2**]FSA was synthesized via the same method using [**1**]FSA (pale-yellow solid, 58% yield). ^{1}H NMR (400 MHz, $CDCl_3$): δ = 3.54 (s, 18H, S(CH_3)$_2$), 5.34 (s, 5H, Cp-H_5). FT-IR (cm^{-1}): 569, 631, 681, 716, 832, 967, 1021, 1082, 1179, 1190, 1379, 2926, 3011, 3119. Anal. Calcd. for: $C_{11}H_{23}F_2NO_7RuS_5$: C, 22.75, H, 3.99, N, 2.41. Found: C, 23.08, H, 3.91, N, 2.40.

4.2.4. *[2]PF_6*

A solution of [Ru(Cp)(CH_3CN)$_3$]PF_6 (29 mg, 0.07 mmol) in DMSO (0.5 mL) was stirred for 16 h at 40 °C in a nitrogen atmosphere, and the solvent was removed under vacuum at 80 °C for 3 h. The reprecipitation of the product from acetone–diethyl ether (−40 °C) thrice afforded the desired compound as a pale-yellow solid (26 mg, 70% yield). ^{1}H NMR (400 MHz, $CDCl_3$): δ = 3.53 (s, 18H, S(CH_3)$_2$), 5.30 (s, 5H, Cp-H_5). FT-IR (cm^{-1}): 681, 720, 832, 924, 961, 1017, 1028, 1094, 1321, 1418, 2930, 3019, 3111. Anal. Calcd. for $C_{11}H_{21}F_6O_3PRuS_3$: C, 24.22; H, 4.25; N, 0. Found: C, 24.53; H, 4.33; N, 0.08.

4.3. X-ray crystallography

Single crystals of [**1**]CPFSA, [**1**]$SbCl_{6,\ [2]CPFSA}$, [**2**]FSA, and [**2**]PF_6 grown by recrystallization from acetone–diethyl ether (−40 °C or −6 °C) were used for structure analysis. XRD data were collected using a Bruker APEX II Ultra (X-ray source: MoKα). The calculations were performed using SHELXL [35], and Tables S1 and S2 list the crystallographic parameters. CCDC 2239501 ([**1**]CPFSA, 90 K), 2263578 ([**1**]$SbCl_6$, 90 K), 2242114 ([**2**]CPFSA, 90 K), 2282354 ([**2**]FSA, 90 K), and 2050269 ([**2**]PF_6, 90 K) contain supplementary crystallographic data for this study.

CRediT authorship contribution statement

Ryota Inoue: Writing – original draft, Visualization, Investigation. **Ryo Sumitani:** Investigation. **Tomoyuki Mochida:** Writing – review & editing, Writing – original draft, Investigation, Conceptualization.

Declaration of competing interest

The authors declare that they have no known competing financial interests or personal relationships that could have appeared to influence the work reported in this paper.

Data availability

Data will be made available on request.

Acknowledgement

We thank Y. Okada for his help with the preparation of [**2**]PF_6. This work was financially supported by KAKENHI (grant number: 22K19049) from the Japan Society for the Promotion of Science (JSPS).

Supplementary materials

Supplementary material associated with this article can be found, in the online version, at doi:10.1016/j.jorganchem.2024.123162.

References

[1] H. Zhu, D.R. MacFarlane, J.M. Pringle, M. Forsyth, Organic ionic plastic crystals as solid-state electrolytes, Trends Chem 1 (2019) 126–140.

[2] A. Kobayashi, J. Yamagami, S. Ranjan, S. Takamizawa, H. Honda, Solid state ^{1}H, ^{7}Li, and ^{13}C NMR studies on new ionic plastic crystals of crown ether-Li-TFSA complexes, Phys. Chem. Chem. Phys. 25 (2023) 27836–27847.

[3] S. Das, A. Mondal, C.M. Reddy, Harnessing molecular rotations in plastic crystals: a holistic view for crystal engineering of adaptive soft materials, Chem. Soc. Rev. 49 (2020) 8878–8896.

[4] D.R. MacFarlane, J. Huang, M. Forsyth, Lithium-doped plastic crystal electrolytes exhibiting fast ion conduction for secondary batteries, Nature 402 (1999) 792–794.

[5] M.L. Thomas, K. Hatakeyama-Sato, S. Nanbu, M. Yoshizawa-Fujita, Organic ionic plastic crystals: flexible solid electrolytes for lithium secondary batteries, Energy Adv. 2 (2023) 748–764.

[6] H.-Y. Zhang, Y.-Y. Tang, P.-P. Shi, R.-G. Xiong, Toward the targeted design of molecular ferroelectrics: modifying molecular symmetries and homochirality, Acc. Chem. Res. 52 (2019) 1928–1938.

[7] J. Harada, T. Shimojo, H. Oyamaguchi, H. Hasegawa, Y. Takahashi, K. Satomi, Y. Suzuki, J. Kawamata, T. Inabe, Directionally tunable and mechanically deformable ferroelectric crystals from rotating polar globular ionic molecules, Nat. Chem. 8 (2016) 946–952.

[8] J. Harada, H. Takahashi, R. Notsuka, M. Takehisa, Y. Takahashi, T. Usui, H. Taniguchi, Ferroelectric ionic molecular crystals with significant plasticity and a low melting point: high performance in hot-pressed polycrystalline plates and melt-grown crystalline sheets, Angew. Chem. Int. Ed. 62 (2023).

[9] Z.-H. Wei, Z.-T. Jiang, X.-X. Zhang, M.-L. Li, Y.-Y. Tang, X.-G. Chen, H. Cai, R.-G. Xiong, Rational design of ceramic-like molecular ferroelectric by quasi-spherical theory, J. Am. Chem. Soc. 142 (2020) 1995–2000.

[10] E.D. Sødahl, J. Walker, K. Berland, Piezoelectric response of plastic ionic molecular crystals: role of molecular rotation, Cryst. Growth Des. 23 (2023) 729–740.

[11] M. Moskwa, E. Ganczar, P. Sobieszczyk, W. Medycki, P. Zieliński, R. Jakubas, G. Bator, Temperature-stimulus responsive ferroelastic molecular–ionic crystal: $(C_8H_{20}N)[BF_4]$, J. Phys. Chem. C. 124 (2020) 18209–18218.

[12] J.-H. Lin, J.-R. Lou, L.-K. Ye, B.-L. Hu, P.-C. Zhuge, D.-W. Fu, C.-Y. Su, Y. Zhang, Halogen engineering to realize regulable multipolar axes, nonlinear optical response, and piezoelectricity in plastic ferroelectrics, Inorg. Chem. 62 (2023) 2870–2876.

[13] A. Basile, M. Hilder, F. Makhlooghiazad, C. Pozo-Gonzalo, D.R. MacFarlane, P. C. Howlett, M. Forsyth, Ionic liquids and organic ionic plastic crystals: advanced electrolytes for safer high performance sodium energy storage technologies, Adv. Energy Mater. 8 (2018) 1703491.

[14] J. Salgado-Beceiro, J.M. Bermúdez-García, A.L. Llamas-Saiz, S. Castro-García, M. A. Señarís-Rodríguez, F. Rivadulla, M. Sánchez-Andújar, Multifunctional properties and multi-energy storage in the $[(CH_3)_3S][FeCl_4]$ plastic crystal, J. Mater. Chem. C. 8 (2020) 13686–13694.

[15] K. Matsumoto, U. Harinaga, R. Tanaka, A. Koyama, R. Hagiwara, K. Tsunashima, The structural classification of the highly disordered crystal phases of $[N_n][BF_4]$, $[N_n][PF_6]$, $[P_n][BF_4]$, and $[P_n][PF_6]$ salts (N_n^+ = tetraalkylammonium and P_n^+ = tetraalkylphosphonium), Phys. Chem. Chem. Phys. 16 (2014) 23616–23626.

[16] R.J. Webb, M.D. Lowery, Y. Shiomi, M. Sorai, R.J. Wittebort, D.N. Hendrickson, Ferrocenium hexafluorophosphate: molecular dynamics in the solid state, Inorg. Chem. 31 (1992) 5211–5219.

[17] H. Schottenberger, K. Wurst, U.J. Griesser, R.K.R. Jetti, G. Laus, R.H. Herber, I. Nowik, ^{57}Fe-labeled octamethylferrocenium tetrafluoroborate. X-ray crystal structures of conformational isomers, hyperfine interactions, and spin-lattice relaxation by Moessbauer spectroscopy, J. Am. Chem. Soc. 127 (2005) 6795–6801.

[18] F. Grepioni, G. Cojazzi, S.M. Draper, N. Scully, D. Braga, Crystal forms of hexafluorophosphate organometallic salts and the importance of charge-assisted C—H—F hydrogen bonds, Organometallics 17 (1998) 296–307.

[19] H. Kimata, T. Mochida, Effects of molecular structure on phase transitions of ionic plastic crystals containing cationic sandwich complexes, Cryst. Growth Des. 18 (2018) 7562–7569.

[20] H. Kimata, T. Sakurai, H. Ohta, T. Mochida, Phase transitions, crystal structures, and magnetic properties of ferrocenium ionic plastic crystals with CF_3BF_3 and other anions, ChemistrySelect 4 (2019) 1410–1415.

[21] H. Kimata, T. Mochida, Phase transitions and crystal structures of organometallic ionic plastic crystals comprised of ferrocenium cations and CH_2BrBF_3 anions, J. Organomet. Chem. 895 (2019) 23–27.

[22] T. Mochida, Y. Funasako, T. Inagaki, M.-J. Li, K. Asahara, D. Kuwahara, Crystal structures and phase-transition dynamics of cobaltocenium salts with bis (perfluoroalkylsulfonyl)amide anions: remarkable odd-even effect of the fluorocarbon chains in the anion, Chem. Eur. J. 19 (2013) 6257–6264.

[23] T. Mochida, M. Ishida, T. Tominaga, K. Takahashi, T. Sakurai, H. Ohta, Paramagnetic ionic plastic crystals containing the octamethylferrocenium cation: counteranion dependence of phase transitions and crystal structures, Phys. Chem. Chem. Phys. 20 (2018) 3019–3028.

[24] T. Mochida, R. Sumitani, T. Yamazoe, Thermal properties, crystal structures, and phase diagrams of ionic plastic crystals and ionic liquids containing a chiral cationic sandwich complex, Phys. Chem. Chem. Phys. 22 (2020) 25803–25810.

[25] T. Mochida, Y. Funasako, M. Ishida, S. Saruta, T. Kosone, T. Kitazawa, Crystal structures and phase sequences of metallocenium salts with fluorinated anions: effects of molecular size and symmetry on phase transitions to ionic plastic crystals, Chem. Eur. J. 22 (2016) 15725–15732.

[26] T. Tominaga, T. Ueda, T. Mochida, Effect of substituents and anions on the phase behavior of Ru(II) sandwich complexes: exploring the boundaries between ionic liquids and ionic plastic crystals, Phys. Chem. Chem. Phys. 19 (2017) 4352–4359.

[27] F. Grepioni, G. Cojazzi, D. Braga, E. Marseglia, L. Scaccianoce, B.F.G. Johnson, Crystal architecture of the cocrystalline salt $[Ru(\eta^5\text{-}C_5H_5)(\eta^6\text{-trans-PhCH=CHPh})][PF_6]\cdot 0.5$trans-PhCH=CHPh and the reversible order–disorder phase transition in $[Ru(\eta^5\text{-}C_5H_5)(\eta^6\text{-}C_6H_6)][PF_6]$, J. Chem. Soc., Dalton Trans. (1999) 553–558.

[28] P. Atkins, T. Overton, J. Rourke, M. Weller, Shriver and Atkins' Inorganic Chemistry, F., Oxford University Press, Oxford, 2010.

[29] A.L. Rohl, D.M.P. Mingos, Size and shape of molecular ions and their relevance to the packing of the 'soft salts, Inorganica Chim. Acta 212 (1993) 5–13.

[30] J.A. Davies, The coordination chemistry of sulfoxides with transition metals, Adv. Inorg. Chem. 24 (1981) 115–187.

[31] J.J. Rack, N.V. Mockus, Room-temperature photochromism in cis- and trans-$[Ru(bpy)_2(dmso)_2]^{2+}$, Inorg. Chem. 42 (2003) 5792–5794.

[32] M.K. Smith, J.A. Gibson, C.G. Young, J.A. Broomhead, P.C. Junk, F.R. Keene, Photoinduced ligand isomerization in dimethyl sulfoxide complexes of ruthenium (II), Eur. J. Inorg. Chem. 2000 (2000) 1365–1370.

[33] K. Matsumoto, T. Oka, T. Nohira, R. Hagiwara, Polymorphism of alkali bis (fluorosulfonyl)amides ($M[N(SO_2F)_2]$, M = Na, K, and Cs), Inorg. Chem. 52 (2013) 568–576.

[34] PDXL2: Integrated X-ray Powder Diffraction Software, Version 2.8.4.0, Rigaku, Tokyo, Japan, 2011.

[35] G.M. Sheldrick, A short history of SHELX, Acta Crystallogr. A 64 (2008) 112–122.